HiSST: 3rd International Conference on
High-Speed Vehicle Science Technology
14 -19 April 2024, Busan, Korea

# A 3D Parallel Lagrangian Finite Volume Scheme for Ideal MHD Equations

*Xiao Xu[1], Hongbo Lu[1], Jian Lin[1], Feng Ji[1] and Nong Chen[1]*

## Abstract

MHD is widely applied in the area of hypersonic flow control, fusion energy, celestial physics and so on. This paper presents a 3D parallel Lagrangian scheme on unstructured meshes for ideal MHD equations. As the meshes move along with the fluids in Lagrangian computation, this method would capture and describe the material interface and shock discontinuities automatically and precisely. Based on the geometry conservation, momentum and total energy conservation and magnetic flux conservation, a compatible nodal approximate Riemann solver is constructed via discrete entropy inequality. The conservative variables are piecewise linear reconstructed to increase spatial discretization accuracy and predictor-corrector time discretization method is adopted in our scheme. The magnetic divergence constraint is satisfied by using the generalized Lagrangian multiplier method, which propagates and dissipates the magnetic divergence error to the computation boundaries. Moreover, parallel computing is conducted on our scheme by exchange information of the boundary cells of each neighbouring block. Various numerical tests verify and validate the accuracy and robustness of our scheme.

**Keywords:** *MHD, Lagrangian Method, Riemann Solver, Magnetic Divergence, Parallel Computing.*

## 1. Introduction

Numerical simulation of MHD is widely used in the area of hypersonic flow control, celestial physics, confined fusion and so on, it can give detailed evolution process and clear flow characteristics of plasma which are difficult to obtain by experiments or physical analysis. However, the MHD govern system which combined Naiver−Stokes equations together with the Maxwell equations is nonlinear hyperbolic, and the wave structure is much more complicated than that in hydrodynamic system. For simplicity, researchers usually concern about the ideal MHD equations where the effects of resistivity, thermal conductivity and viscosity are ignored.

Most numerical methods for ideal MHD equations are based on Eulerian mesh framework, thus the computational meshes are fixed all the time and we compute the numerical flux on the boundary of the each mesh and then conduct time and spatial evolution of the discrete hyperbolic conservation systems. Another type of mesh based method, which deals with solving the partial differential equations the on the moving meshes, is Lagrangian method or arbitrary Lagrangian Eulerian method[1]. As the meshed move along with the fluid, thus accurate and sharp interfaces are obtained in Lagrangian method. However, the discreatization of the conservation laws is difficult since the meshes are deformed and moved, which is not simple and straightforward as that performed in Eulerian meshes[2-4].

Another difficulty is to ensure the magnetic divergence free constraint in Lagrangian computation. The divergence of magnetic field is free in physics, but the discrete of $\nabla \cdot B$ is usually not exactly zero in numerical simulations. Besides, these $\nabla \cdot B$ errors may increase with time which will cause unphysical results. Up to now, there are mainly four popular approaches to solve this problem

[1] *China Academy of Aerospace Aerodynamics, 17#, Yungang West Road, Fengtai District, Beijing. xuxiaomelody@126.com.*

including (1) the projection method [8], (2) the non-conservative eight wave method [9], (3) the hyperbolic divergence cleaning method [4], and (4) the constrained transport method [10]. All these methods have been applied to MHD simulations successfully, while each has their own drawbacks [6].

In this paper, we will propose a 3D parallel Lagrangian method for ideal MHD equations. The outline of this paper is as follows. We first introduce the ideal MHD govern equations and the compatible discrete Lagrangian framework in Section 2, In Section 3 the 3D parallel cell-centered Lagrangian scheme for MHD is built, in which the construction of nodal solver, time step control as well as the magnetic divergence cleaning method is presented. The accuracy and the robustness of this Lagrangian scheme are assessed in Section 4 against several classical MHD numerical tests. The conclusion and the future work is given in Section 5.

## 2. Governing equations and operators discretization

### 2.1. Governing equations

The 3D ideal MHD equations consist of a set of nonlinear hyperbolic equations

$$\partial_t \rho + \nabla \cdot (\rho U) = 0,$$

$$\partial_t (\rho U) + \nabla \cdot (\rho UU + P_t \mathrm{I} - BB^T) = 0,$$

$$\partial_t B + \nabla \cdot (UB^T - BU^T) = 0,$$

$$\partial_t (\rho E) + \nabla \cdot [(\rho E + P_t)U - B(U \cdot B)] = 0$$

together with the additional divergence free constraint

$$\nabla \cdot B = 0.$$

Here $\mathrm{B} = \left(\mathrm{B_x}, \mathrm{B_y}, \mathrm{B_z}\right)^{\mathrm{T}}$ and $\mathrm{U} = \left(\mathrm{U_x}, \mathrm{U_y}, \mathrm{U_z}\right)^{\mathrm{T}}$ denote the magnetic induction and the fluid velocity respectively. $\mathrm{I}$ denotes the $3 \times 3$ unit matrix, $\rho$ is the fluid density, $\mathrm{P_t}$ is the total pressure of magnetic fluid and $\mathrm{E}$ is the specific total energy of magnetic fluid,

$$P_t = p + p_b = p + \frac{1}{2}|B|^2,$$

$$E = \varepsilon + \frac{1}{2}|U|^2 + \frac{1}{2\rho}|B|^2,$$

and the hydrodynamic pressure p is given by the state equation $\mathrm{p} = \mathrm{p}(\rho, \varepsilon)$. It should be noted that the proposed method in this paper is suitable for the general equations of state, and for simplicity we assume the gas to be perfect

$$p = (\gamma - 1)\rho\varepsilon,$$

where an adiabatic exponent $\gamma > 1$. This system combines the equations of gas dynamics with the Maxwell equations for problems in which relativistic, viscous, resistive effects can be neglected and the permeability is set to unity.

Now we induce the material derivative $\frac{\mathrm{df}}{\mathrm{dt}} = \frac{\partial \mathrm{f}}{\partial \mathrm{t}} + \mathrm{U} \cdot \nabla \mathrm{f}$, and we obtain the updated-type Lagrangian formalism of the ideal MHD equations as follows

$$\rho \frac{d\tau}{dt} = \nabla \cdot U, \tag{1}$$

$$\rho \frac{dU}{dt} = -\nabla \cdot (P_t I - BB^T), \tag{2}$$

$$\rho \frac{d(\tau B)}{dt} = \nabla \cdot (BU), \tag{3}$$

$$\rho \frac{dE}{dt} = -\nabla \cdot [P_t U - B(U \cdot B)], \tag{4}$$

here $\tau = 1/\rho$ is the specific volume. As the Lagrangian meshes move along with the fluid, an additional trajectory equation is then introduced to describe the motion of a node x

$$\frac{dx}{dt} = U, \tag{5}$$

with initial condition $\mathrm{x}(\mathrm{t}=0)=\mathrm{x}_0$. Eqs. (1) – (5) together determine the flow characteristics of magnetic fluid and we will discretize them later.

### 2.2. The discretization of divergence operator and gradient operator

In this paper, the meshes are discretized with the method proposed by Georges et al. For the completeness, we just briefly give the derivative process and main results, the readers can refer to [1] to get the details of this method. We firstly split the cell faces into a set of triangles with the help of an additional point $\mathrm{p}_\mathrm{f}^*$ in each face, here the additional point is just defined at the center of this face, see in Fig. 1.

After the faces splitting, we combine all split triangles with each cell center and then get a full tetrahedral decomposition of the spatial domain $\omega(\mathrm{t})$. We use c, f and p which denote a cell, a face and a node respectively. we look back the mass conservation equation and substitute the mass m of fluid into Eq. (1), we can easily get

$$\frac{1}{v_c}\frac{dv}{dt}=\nabla\cdot\boldsymbol{U}, \tag{6}$$

Eq. (6) is nothing but geometry conservation law which indicates that the unit cell volume time rate of change must be equal to the cell velocity divergence during the Lagrangian computation. By discretizing GCL equation (6), the detailed procedure can refer to our previous work[2,3], we introduce the corner face area vector $\mathrm{S_{pf}n_{pf}}$, then the divergence operator and gradient operator in the finite volume can be derived as

$$(\nabla\cdot\psi)_{\omega_c}=\frac{1}{v_c}\sum_{p\in P(c)}\sum_{f\in F(c,p)}\psi_p\cdot S_{pf}\mathbf{n}_{pf}\,, \tag{7}$$

$$(\nabla\phi)_{\omega_c}=\frac{1}{v_c}\sum_{p\in P(c)}\sum_{f\in F(c,p)}\phi_p S_{pf}\mathbf{n}_{pf}\,, \tag{8}$$

where $\psi$ and $\phi$ are any vector and scalar in the cell $\omega_\mathrm{c}$ respectively, $\psi_\mathrm{p}$ and $\phi_\mathrm{p}$ are the corresponding nodal values.

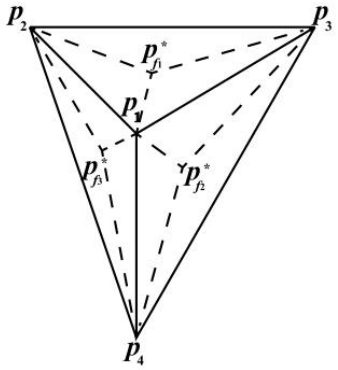


**Fig 1.** Result of the splitting of the cell faces into triangles using the supporting node $\mathrm{p}_\mathrm{f}^*$. Simple case of a tetrahedral cell with triangular faces.

## 3. Construction of the scheme

### 3.1. Discretization of the updated-type Lagrangian equations

In a Lagrangian scheme, the mass conservation equation is automatically fulfilled since the mass m is constant in each cell. Now apply the previous discrete operators (7) and (8) in (2)–(4),

$$m\frac{d\boldsymbol{U}}{dt}=-\sum_{p\in P(c)}\sum_{f\in F(c,p)}S_{pf}p_{cfp}\mathbf{n}_{pf}+\sum_{p\in P(c)}\sum_{f\in F(c,p)}S_{pf}\mathbf{n}_{pf}\cdot\left(\boldsymbol{B}_p\boldsymbol{B}_p\right), \tag{9}$$

$$m\frac{d(\tau\boldsymbol{B})}{dt}=\sum_{p\in P(c)}\sum_{f\in F(c,p)}S_{pf}\mathbf{n}_{pf}\cdot\left(\boldsymbol{B}_p\boldsymbol{U}_p\right), \tag{10}$$

$$m\frac{dE}{dt}=-\sum_{p\in P(c)}\sum_{f\in F(c,p)}S_{pf}p_{cfp}\boldsymbol{U}_p\cdot\mathbf{n}_{pf}+\sum_{p\in P(c)}\sum_{f\in F(c,p)}S_{pf}\mathbf{n}_{pf}\cdot\left[\boldsymbol{B}_p\left(\boldsymbol{U}_p\cdot\boldsymbol{B}_p\right)\right], \tag{11}$$

here the subscript c denotes the cell-averaged quantities while the subscript p denotes the nodal quantities. $p_{cfp}$ is the nodal pressure flux which defined on the nodes. Moreover, the GCL equation (6) and magnetic divergence free constraint can be also written as

$$\frac{dv_c}{dt} = \sum_{p\in P(c)} \sum_{f\in F(c,p)} S_{pf}\mathbf{n}_{pf} \cdot \boldsymbol{U}_p\,, \tag{12}$$

$$\nabla \cdot B_c = \frac{1}{v_c}\sum_{p\in P(c)} \sum_{f\in F(c,p)} \boldsymbol{B}_p \cdot S_{pf}\mathbf{n}_{pf} = 0. \tag{13}$$

### 3.2. Entropy inequality

Considering the entropy of a cell, the temperature and entropy are denoted by $\theta_c$ and $\eta_c$ respectively. The Gibbs relation writes

$$m\theta_c \frac{d\eta_c}{dt} = m\frac{d\varepsilon_c}{dt} + p\frac{dv_c}{dt},$$

apply the semi-discrete equations (9)–(13) into above equality with some transformations, it yields

$$m\theta_c \frac{d\eta_c}{dt} = \sum_{p\in P(c)} \sum_{f\in F(c,p)} S_{pf}(p_{cfp} - P_t)(\boldsymbol{U}_c - \boldsymbol{U}_p)\cdot \mathbf{n}_{pf} - \sum_{p\in P(c)} \sum_{f\in F(c,p)} S_{pf}(\mathbf{n}_{pf}\cdot \boldsymbol{B}_p)\cdot\left[(\boldsymbol{U}_c - \boldsymbol{U}_p)\cdot(\boldsymbol{B}_p - \boldsymbol{B}_c)\right]$$

in order to satisfy the non-decreasing condition of entropy, one obtains

$$(\boldsymbol{U}_c - \boldsymbol{U}_p)\cdot\left[(p_{cfp} - P_t)\mathbf{n}_{pf} - (\boldsymbol{B}_p - \boldsymbol{B}_c)(\mathbf{n}_{pf}\cdot\boldsymbol{B}_p)\right] \geq 0,$$

Here, a sufficient condition for the above inequality is

$$(p_{cfp} - P_t)\mathbf{n}_{pf} - (\boldsymbol{B}_p - \boldsymbol{B}_c)(\mathbf{n}_{pf}\cdot\boldsymbol{B}_p) = Z_c(\boldsymbol{U}_c - \boldsymbol{U}_p),$$

thus the pressure jump is expressed in terms of velocity jump and magnetic induction jump as follows

$$p_{cfp} = P_t + \left[(\boldsymbol{B}_p - \boldsymbol{B}_c)\cdot\mathbf{n}_{pf}\right](n_{pf}\cdot\boldsymbol{B}_p) + Z_c(\boldsymbol{U}_c - \boldsymbol{U}_p)\cdot\mathbf{n}_{pf}, \tag{14}$$

where $Z_c = \rho_c a_c$ denotes the magnetic acoustic impedance defined in cell c, $a_c$ is the fastest magnetosonic speed.

### 3.3. Nodal solver

For an inner node p in the $\omega(t)$, the total energy is conserved, and a sufficient condition is that the sum of forces acting on node p (referring to Fig. 2) is equal to zero,

$$\sum_{c\in C(p)} \sum_{f\in F(c,p)} S_{pf}p_{cfp}\mathbf{n}_{pf} = 0,$$

Substitute (14) into above equality and the nodal approximate Riemann solver is obtained as $U_p = M_p^{-1}L$, where

$$\boldsymbol{M}_p = \sum_{c\in C(p)} \sum_{f\in F(c,p)} S_{pf}Z_c\mathbf{n}_{pf}\mathbf{n}_{pf} = 0,$$

$$\boldsymbol{L} = \sum_{c\in C(p)} \sum_{f\in F(c,p)} S_{pf}\left\{\left[P_t + \left[(\boldsymbol{B}_p - \boldsymbol{B}_c)\cdot\mathbf{n}_{pf}\right](\mathbf{n}_{pf}\cdot\boldsymbol{B}_p)\right]\mathbf{n}_{pf} + Z_c\mathbf{n}_{pf}\mathbf{n}_{pf}\boldsymbol{U}_c\right\}.$$

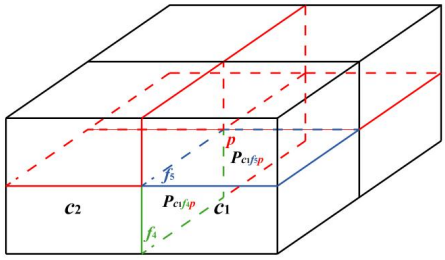

**Fig 2.** Representation of the pressure fluxes $\mathrm{p}_{\mathrm{cfp}}$ acting around a node p, Simple case for structured hexahedrons.

### 3.4. Time step control

The classical predictor-corrector method is utilized for time discretization. For Lagrangian computation, the time step is controlled by CFL criterion and cell volume variation rate limitation, which means the computation cells can not deform too much during the time step

$$\Delta t_v = C_v min \frac{v_c^n}{\frac{dv_c^n}{dt}}.$$

### 3.5. Magnetic divergence free treatment

In this paper, we use the generalized Lagrangian multiplier method the deal with the magnetic divergence error. First we introduce a linear differential operator D and scalar function $\varphi$ to combine the magnetic field evolution equation (3) together with the magnetic divergence constraint,

$$\rho \frac{d(\tau \boldsymbol{B})}{dt} = \nabla \cdot (\boldsymbol{BU} - \varphi \boldsymbol{I}),$$
$$D(\varphi) + \nabla \cdot \boldsymbol{B} = 0.$$

Previous work[4] proved that $\nabla \cdot \mathrm{B}$ and $\varphi$ satisfy the same equation for any choice of D. Here we choose D as $\mathrm{D}(\varphi) = \frac{1}{c_h^2}\partial_t \varphi + \frac{1}{c_p^2}\varphi$, thus the magnetic divergence constraint is then transformed as

$$\partial_t \varphi + c_h^2 \nabla \cdot \boldsymbol{B} = -\frac{c_h^2}{c_p^2}\varphi,$$

which can be solved explicitly.

### 3.6. Parallel computing

As the algorithm for ideal MHD equations we proposed is based on 3D unstructured meshes, the parallelism for the large scale program is quite difficult. According to the MPI framework, we study and program the entire modules for parallelism, including the unstructured subdomain decomposition, the data exchange between processes, the parallel input/output and so on. Moreover, since our scheme for MHD equations is explicit, it would accomplish quite high parallel computing efficiency.

## 4. Numerical tests

In this section, several HD/MHD examples will shown the accuracy, robustness and efficiency of the proposed Lagrangian method.

### 4.1. Brio–Wu shock tube test

This standard test is an extension of the classical Sod problem to MHD and was first introduced by Brio and Wu [5]. The initial condition is given as

$$\left(\rho, U_x, U_y, U_z, B_y, B_z, p\right) = \begin{cases} (1, 0, 0, 0, 1, 0, 1), & if\ x \le 0 \\ (0.125, 0, 0, 0, -1, 0, 0.1), & if\ x > 0 \end{cases}$$

with $\mathrm{B}_{\mathrm{x}} = 0.75$. The computational domain is $[-1, 1] \times [-0.3, 0.3] \times [0, 0.1]$ which is divided into $800 \times 240 \times 2$ hexahedral cells. At t = 0, the initial discontinuity is at x = 0. The final time is set to 0.25 and $\gamma = 2$.

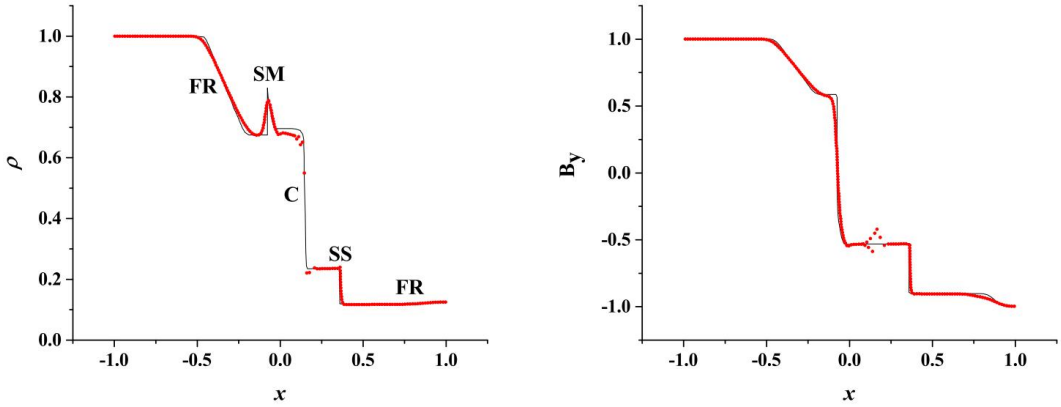


**Fig 3.** Solutions of Brio–Wu shock tube test. In the figure of ρ, FR denotes a fast rarefaction wave, SM denotes a slow compound wave, C denotes a contact discontinuity and SS denotes a slow shock.

Fig 3 presents the solution of $\rho$, $B_y$ respectively. From the result of $\rho$ we can see the rarefaction wave, compound wave, contact discontinuity, shock and rarefaction wave from left to right. This compound wave is formed as $B_y = 0$ (and $B_z = 0$), where the MHD system hits a degenerate point and the solution switches from a overcompressive shock to a rarefaction wave. Although there exist some small numerical oscillations after the contact discontinuity and shock wave, our results plotted in red scatters fit well from that in [6].

### 4.2. 2D MHD rotor test

This classical MHD problem was first documented in Balsara [7] and then tested for comparison of different schemes by Toth [35]. It describes the interaction of a rotating vortex with the ambient static fluid under a initially uniform magnetic field. Here we take the same test as [35], these initial conditions are

$$\rho = \begin{cases} 10, & if\ r \le 0.1; \\ -600r + 70, & if\ 0.1 < r \le 0.115; \\ 1, & if\ r > 0.115. \end{cases}$$

$$V_x = \begin{cases} -20y, & if\ r \le 0.1; \\ -(46 - 400r)y/3, & if\ 0.1 < r \le 0.115; \\ 0, & if\ r > 0.115. \end{cases}$$

$$V_y = \begin{cases} 20x, & if\ r \le 0.1; \\ (46 - 400r)x/3, & if\ 0.1 < r \le 0.115; \\ 0, & if\ r > 0.115. \end{cases}$$

The computational domain is $[-0.5, 0.5] \times [-0.5, 0.5] \times [0, 0.2]$, and $50 \times 50 \times 2$ uniform hexahedral meshes are divided in this simulation. Symmetry boundary conditions are imposed in this case and the the final time is set to t = 0.15 with the adiabatic index $\gamma = 1.4$.

Fig 4 shows the results of density, thermal pressure, magnetic pressure and magnitude of magnetic field at t=0.15 for the 2D MHD rotor test at slice z = 0.1 with 50 equally spaced contours respectively. We also note that the magnetic field lines rotate with the fluid in the center which is in conformity with the conservation of the magnetic flux, while minor error exists near the boundary of the domain, this is because the center divergence error transport to the boundary at the end time, which leads to a non-zero value of $\psi$, thus a disturbance of the magnetic fields occurs where the magnetic field line is not exactly horizontal.

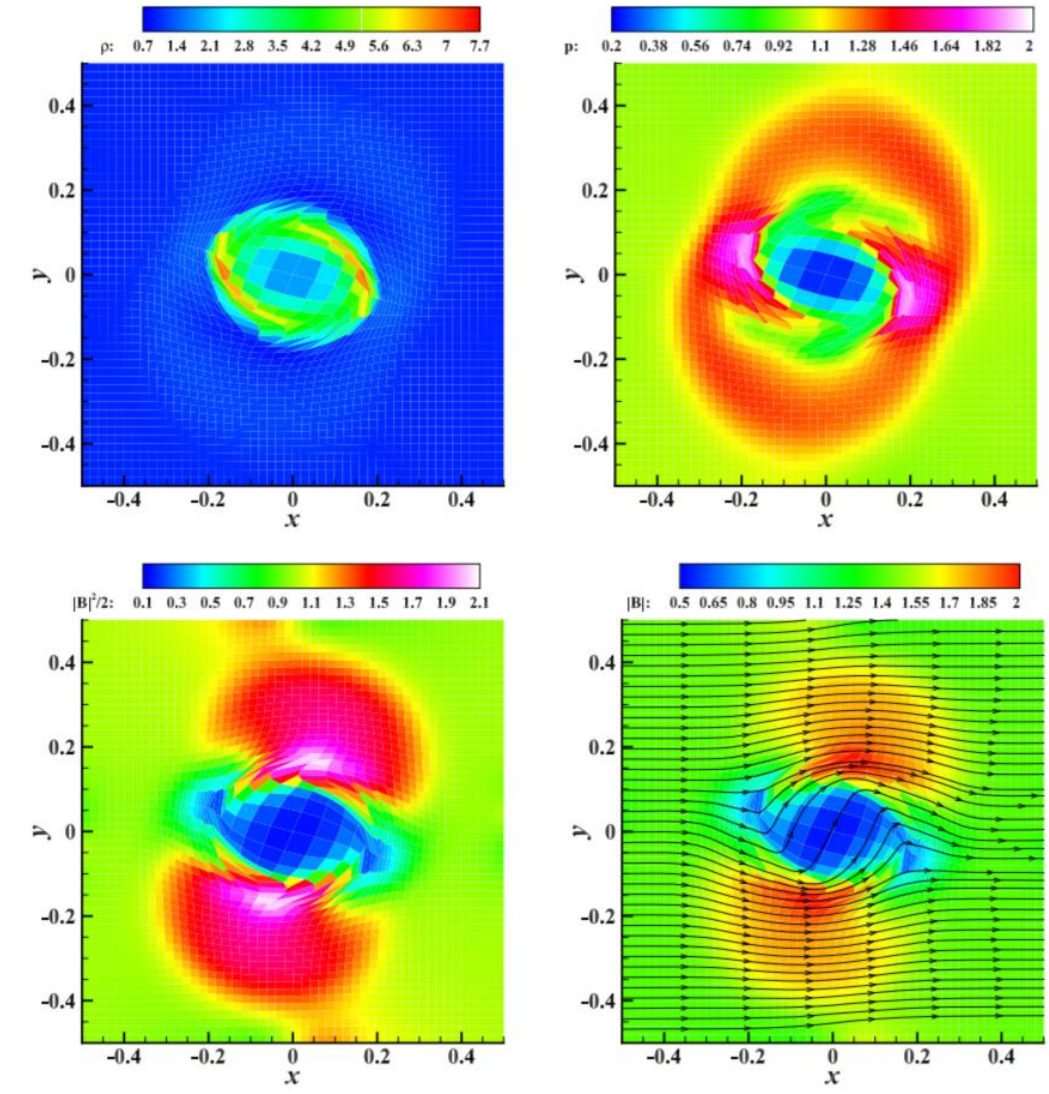


**Fig 4.** The density, thermal pressure, magnetic pressure and magnitude of magnetic field at t=0.15 for the 2D MHD rotor test.

### 4.3. 3D blast test

This test is proposed to validate the accuracy of the algorithm for hydrodynamics. There exists a high energy $e = 0.106384$ at the origin of the initial unit cubic domain, for the rest of the domain, the initial internal energy is set to $2.5 \times 10^{-6}$. The fluid is static with unit density at the initial time, as the local center internal energy transforms to kinetic energy, a strong spherical shock wave generates and propagates outward in the domain. The end time for this test is 1.0 and the meshes we use for this test are 40×40×40 hexahedrons and parallel computing is conducted in this test.

Fig 5 shows the density results of the 3D blast test at the end time, we use 8 processors to parallel compute the problem. In the middle of Fig 5 shows the density contours of processors 2~8 and results of the remaining processor 1 is shown on the right. Table 1 further presents the computing time and the responding parallel efficiency for the test. We can see the parallel program can reach as high as a hundred percent of parallel efficiency, as the meshes in this test are of small scale, when the number of processors is 16, the time lost caused by the MPI data exchange diminishes the parallel efficiency.

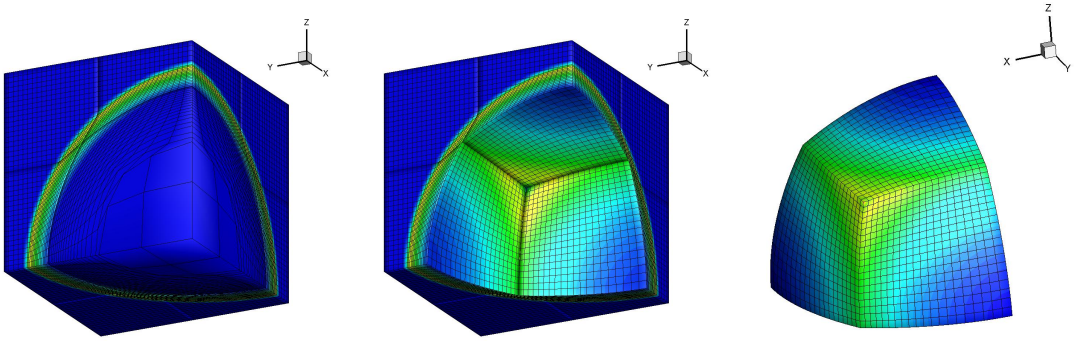

**Fig 5.** The whole density contour(left), processor 2~8 results(middle) and processor 1 result of density(right) for the 3D HD blast test.

**Table 1.** Computing time and the parallel efficiency for the 3D blast test.

| **Processors numbers** | 2 | 4 | 8 | 16 |
|---|---|---|---|---|
| **Computing time** | 688s | 333s | 181s | 110s |
| **parallel efficiency** | 1 | 103% | 95% | 78% |

### 4.4. 3D MHD blast test

This 3D MHD blast test is taken from [7] by Balsara. The problem consists of a $\gamma = 1.4$ gas with a unit density and a pressure of 0.1 initialized on a cubic domain $[-0.5, 0.5]\times[-0.5, 0.5]\times[-0.5, 0.5]$. In the center of the domain, the pressure is reset a value of 1000 within the radius $r < 0.1$. The gas is static at $t = 0$ under a constant magnetic field $B_x = B_y = B_z = 50/\sqrt{3}/\sqrt{4\pi}$. The problem is run up to a time of 0.012, by which time a strong magnetosonic blast wave propagates though the domain. The meshes we use for this test are $100\times100\times100$ hexahedrons and parallel computing is conducted in this test.

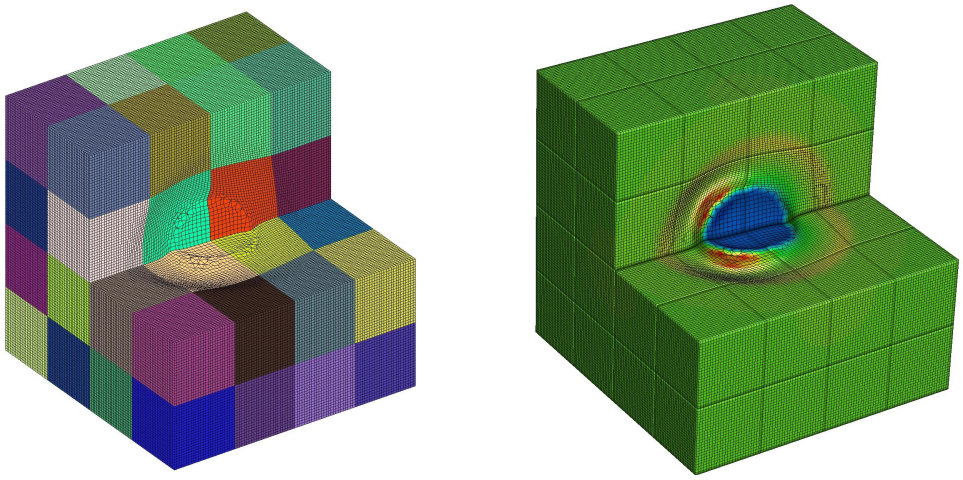

**Fig 6**. The Lagrangian meshes(left) and distribution of density(right) at t = 0.012 for the 3D MHD blast test.

Fig 6 shows the Lagrangian meshes and the density contour in 3D at t = 0.012 for this test. As the Lorentz force acts vertically on the flow velocity direction, thus the explosive shock waves are stretched. We extract the values of density, velocity, magnetic field and pressure along the diagonal line of the computational domain, the results are consistent with the solutions given in [7].Table 2 further presents the computing time and the responding parallel efficiency for the test. We can see the parallel can obviously reduce the computing time for the test, still as the number of processors increases, the time lost caused by the MPI data exchange diminishes the parallel efficiency.

**Table 2.** Computing time and the parallel efficiency for the 3D MHD blast test.

| **Processors numbers** | 1 | 8 | 16 | 32 | 64 |
|---|---|---|---|---|---|
| **Computing time** | 47887s | 6477s | 3488s | 1841s | 1065s |
| **parallel efficiency** | 1 | 92% | 86% | 81% | 70% |

## 5. Conclusion

In this paper we propose a parallel Lagrangian scheme to solve the 3D ideal MHD equations. All the variables are compatibly discredized in the finite volume to meet the GCL requirement. By introducing a Lagrange multiplier, the magnetic divergence constraint is coupled with the conservation laws. This method is validated to control the magnetic divergence effectively, meanwhile the whole GLM-MHD system is fully explicit hence the parallelism of the programme is easy to conduct, and the parallel computation efficiency is then tested. Moreover, the numerical results are comparable to those of Eulerian or ALE schemes even for some very stringent test problems, which validate the accuracy and robustness of our scheme.

## References


1. G. Georges, J. Breil, P.H. Maire, A 3D GCL compatible cell-centered Lagrangian scheme for solving gas dynamics equations, J. Comput. Phys. 305 (2016) 921–941.
2. Xiao Xu, Zihuan Dai and Zhiming Gao. A 3D cell-centered Lagrangian scheme for the ideal Magnetohydrodynamics equations on unstructured meshes, Comput. Methods Appl. Mech. Engrg, 342: 490-508(2018).
3. Xiao Xu, Guoxi Ni. A Finite Volume Method for the 3D Lagrangian Ideal Compressible Magnetohydrodynamics. J. Sci. Comput., 91:73 (2022).
4. A. Dedner, F. Kemm, D. Kroner, et al., Hyperbolic divergence cleaning for the MHD equations, J. Comput. Phys. 175 (2002) 645–673.
5. M. Brio, C.C. Wu, An upwind difference scheme for the equations of ideal magnetohydrodynamics, J. Comput. Phys. 75 (1988) 400–422.
6. M. Wesenburg, Efficient MHD Riemann solvers for simulations on unstructured triangular grids, J. Numer. Math. 10 (2002) 37–71.
7. D. S. Balsara, Self-adjusting, positivity preserving high order schemes for hydrodynamics and magnetohydrodynamics, J. Comput. Phys. 231(2012) 7504–7517.
8. J. U. Brackbill, D. C. Barnes, The effect of nonzero $\nabla \cdot B$ on the numerical solution of the magnetohydrodynamic equations, J. Comput. Phys. 35 (1980) 426–430.
9. K. G. Powell, An Approximate Riemann Solver for Magnetohydrodynamics (That Works in More than One Dimension), ICASE-Report 94-24, NASA Langley Research Center, Hampton, VA, 1994.
10. C. R. Evans, J. F. Hawley, Simulation of magnetohydrodynamic flowsa constrained transport method, Astrophys. J. 332 (1988) 659–677.


 